Selective inhibition of the p38α MAPK–MK2 axis inhibits inflammatory cues including inflammasome priming signals

Chun Wang[1], Susan Hockerman[2] , E. Jon Jacobsen[2], Yael Alippe[1], Shaun R. Selness[2], Heidi R. Hope[2] , Jeffrey L. Hirsch[2], Stephen J. Mnich[2], Matthew J. Saabye[2], William F. Hood[2], Sheri L. Bonar[2], Yousef Abu-Amer[3], Ariela Haimovich[4], Hal M. Hoffman[4], Joseph B. Monahan[2]*, and Gabriel Mbalaviele[1]*

p38α activation of multiple effectors may underlie the failure of global p38α inhibitors in clinical trials. A unique inhibitor (CDD-450) was developed that selectively blocked p38α activation of the proinflammatory kinase MK2 while sparing p38α activation of PRAK and ATF2. Next, the hypothesis that the p38α–MK2 complex mediates inflammasome priming cues was tested. CDD-450 had no effect on NLRP3 expression, but it decreased IL-1β expression by promoting IL-1β mRNA degradation. Thus, IL-1β is regulated not only transcriptionally by NF-κB and posttranslationally by the inflammasomes but also posttranscriptionally by p38α–MK2. CDD-450 also accelerated TNF-α and IL-6 mRNA decay, inhibited inflammation in mice with cryopyrinopathy, and was as efficacious as global p38α inhibitors in attenuating arthritis in rats and cytokine expression by cells from patients with cryopyrinopathy and rheumatoid arthritis. These findings have clinical translation implications as CDD-450 offers the potential to avoid tachyphylaxis associated with global p38α inhibitors that may result from their inhibition of non-MK2 substrates involved in antiinflammatory and housekeeping responses.

Introduction

The mechanisms that govern posttranscriptional regulation of inflammasome components are unknown despite advances in transcriptional and posttranslational regulation of these constituents. NF-κB regulates the transcription of pro-IL1β and NLRP3 (Bauernfeind et al., 2009; Segovia et al., 2012) and is activated by IκB kinase 2 (IKK2), which itself is phosphorylated by transforming growth factor (TGF)-β–activated kinase 1 (TAK1; Sakurai, 2012). TAK1 also activates p38α MAPK (p38α; Sakurai, 2012), suggesting that p38α plays a role in inflammasome priming signals. Specific docking domains present in p38α substrates facilitate the binding of these proteins to p38α (Mayor et al., 2007). Relevant p38α substrates include MAPK-activated protein kinase 2 (MK2), p38α-related/activated protein kinase (PRAK), and activating transcription factor 2 (ATF2). Activated MK2 phosphorylates downstream effectors including adenylate-uridylate (AU)-rich element binding proteins such as tristetraprolin and heterogeneous nuclear ribonucleoprotein A0, which modulate the stability of mRNA containing AU-rich elements such as those encoding TNF-α and IL-6 (Taylor et al., 1996; Hitti et al., 2006). Evidence strongly indicates that p38α inflammatory actions are mediated by MK2 (Kotlyarov et al., 1999; Hegen et al., 2006).

IL-1β and IL-18 are overproduced in cryopyrin-associated periodic syndromes (CAPS), a spectrum of autoinflammatory disorders caused by *NLRP3*-activating mutations (Hoffman and Brydges, 2011; de Jesus et al., 2015). Anti–IL-1β biologics are widely used in the treatment of CAPS, but these drugs have drawbacks including high price, the requirement for parenteral administration, the potential for development of resistance, and the lack of efficacy against skeletal lesions (Neven et al., 2010; Rigante et al., 2011; Sibley et al., 2012). IL-1β production is also increased in rheumatoid arthritis (RA), a disease in which TNF-α expression and p38α activity are up-regulated (Rosengren et al., 2005; Mbalaviele and Monahan, 2008; Kolly et al., 2010). We recently reported that TNF-α is also involved in the pathogenesis of cryopyrinopathies (McGeough et al., 2017). Because p38α regulates the expression of multiple inflammatory mediators including IL-1β, IL-6, and TNF-α, inhibition of this kinase should in theory provide superior efficacy compared with targeted blockade of individual factors. Several relatively safe p38α inhibitors were

[1]Division of Bone and Mineral Diseases, Washington University School of Medicine, St. Louis, MO;   [2]Confluence Discovery Technologies, Inc., St. Louis, MO;   [3]Department of Orthopaedic Surgery, Washington University School of Medicine, St. Louis, MO;   [4]Department of Pediatrics, University of California, San Diego, La Jolla, CA.

*J.B. Monahan and G. Mbalaviele contributed equally to this paper;   Correspondence to Gabriel Mbalaviele: gmbalaviele@wustl.edu.

developed to test this principle, but unfortunately, they failed in phase II RA clinical studies for reasons including the lack of sustained efficacy (Hammaker and Firestein, 2010; Genovese et al., 2011; Kyttaris, 2012). Potential explanations for the transient efficacy include limited dosing to avoid toxicity, inadequate distribution to the site of inflammation or pain, down-regulation of antiinflammatory pathways, redundancy in the signaling network, or the inhibition of key proteins that are involved in the feedback regulation of other MAPK pathways. In this regard, inhibition of feedback mechanisms may up-regulate other proinflammatory pathways, resulting in increased inflammation. Thus, there is still a need for the development of a safe and efficacious p38α pathway inhibitor for the treatment of inflammatory diseases including CAPS and RA.

CDD-450 selectively blocks p38α activation of MK2 while sparing the inhibition of other effectors of p38α. CDD-450 inhibits the production of IL-1β, IL-6, and TNF-α and is as efficacious as global p38α inhibitors in decreasing inflammation in disease models. Thus, selective inhibition of the p38α–MK2 complex, which may be desirable from a safety standpoint, is not only achievable pharmacologically but is also efficacious in inhibiting inflammatory diseases in preclinical models.

Results and discussion

Selective inhibition of p38α–MK2 decreases IL-1β, IL-6, and TNF-α production by promoting mRNA instability

CDD-450 (Fig. S1 A) was designed to selectively bind to and inhibit the p38α–MK2 complex. It exhibited decreased potency for inhibiting p38α alone or bound to other substrates as it was at least 700× more potent in inhibiting p38α–MK2 than p38α–PRAK or p38α–ATF2 (Fig. 1, A and B). In contrast, a classical p38α inhibitor, CDD-110, a racemate of PH-797804 (Hope et al., 2009), inhibited p38α–MK2 and p38α–PRAK with similar potency (Fig. 1 C).

The interface between p38α and docked MK2 creates unique binding surfaces near the p38α ATP site and an additional MK2-derived cleft relative to p38α alone (ter Haar et al., 2007). These new surfaces and cleft exhibit suitable properties for targeted drug design (Fig. S1 B). CDD-450 was designed to interact with the p38α and MK2 surfaces of the interface cleft in the docked complex (Fig. S1 C). The CDD-450 MK2 binding region had dissimilar residues relative to PRAK, resulting in the observed differential in inhibitor binding to the two complexes. In contrast, binding interactions of the inhibitor CDD-110 were primarily limited to the p38α surface of the docked complex (Fig. S1 D). Surface plasmon resonance analysis of p38α binding to immobilized MK2 in the presence of CDD-450 demonstrated a stabilization of the complex (increased $t_{1/2}$) relative to p38α–MK2 alone (47.5×) or the p38α–MK2 complex in the presence of CDD-110 (4×; Fig. S1 E). These observations indicate that CDD-450 binds more tightly to and stabilizes p38α–MK2 relative to CDD-110. CDD-450 was also highly selective across the human kinome, displaying >350× potency differential for inhibiting the 193 kinases tested (Fig. S1, F and G). Thus, CDD-450 selectively inhibits the p38α–MK2 inflammatory axis with minimal cross-reactivity for blocking p38α activation of other substrates involved in antiinflammatory

and housekeeping responses. Selective inhibitors of p38α–MK2 have been reported, but their efficacy in disease models was not evaluated (Cumming et al., 2015).

The role of p38α and MK2 in posttranscriptional regulation of IL-1β is not well studied. CAPS offer a model for testing the hypothesis that the p38α–MK2 axis regulates inflammasome priming signals as these disorders are associated with oversecretion of IL-1β and are generally responsive to treatment with biological IL-1 inhibitors (Koné-Paut and Galeotti, 2015). From among these syndromes, neonatal-onset multisystem inflammatory disease (NOMID) is the most severe phenotype (Agostini et al., 2004; de Jesus et al., 2015; Hoffman and Broderick, 2016). To determine whether p38α–MK2 regulates inflammasome priming signals, we used NOMID mice expressing constitutively activated NLRP3 in myeloid cells driven by *lysozyme M-Cre* (Qu et al., 2015; Wang et al., 2017). The phenotype of these mice resembles that of mice globally expressing NLRP3 mutant, although the disease is less severe in mice with myeloid-restricted expression of the transgene (Bonar et al., 2012; Qu et al., 2015; Wang et al., 2017). LPS markedly induced IL-1β, IL-6, and TNF-α mRNA expression in WT and NOMID bone marrow macrophages (BMMs; Fig. 1 D and not depicted); these responses correlated with p38α and MK2 activation (Fig. S2, A and B) and were inhibited by CDD-450 (Fig. 1 D). MK2 phosphorylation peaked at 30 min before returning to baseline levels 180 min after stimulation. CDD-450 inhibited the transient LPS-stimulated MK2 phosphorylation at 15 and 30 min, but it had little effect at 180 min, when MK2 activation returned to baseline state (Fig. S2 B). CDD-450 was not cytotoxic at efficacious concentrations tested in this study (not depicted). This inhibitor crossed over p38β (Fig. S1 F), but the literature overwhelmingly indicates that p38α but not p38β drives inflammation in diseases (Hale et al., 1999; Korb et al., 2006). IL-1β mRNA biosynthesis was also inhibited by a selective IKK2 inhibitor, PHA-408 (Fig. 1 D; Mbalaviele et al., 2009), consistent with NF-κB's role in inflammasome priming signals. LPS stimulated the expression of NLRP3 mRNA and protein (Figs. 1 E and S2 B) and IL-18 mRNA to a lesser degree (Fig. 1 F). Notably, NLRP3 and IL-18 expression was decreased by IKK2 inhibitor (Fig. 1, E and F) but not CDD-450 (Figs. 1 E and S2 B; unpublished data). CDD-450 also had no effect on the expression of NLRP3 interacting partners including the adapter protein ASC, caspase-1, and the kinase NEK7 (not depicted; Broz and Dixit, 2016; Shi et al., 2016; Man et al., 2017).

The role of p38α–MK2 in the stability of IL-1β, TNF-α, IL-6, and NLRP3 transcripts in WT or NOMID BMMs stimulated with LPS was studied. CDD-450 promoted the degradation of IL-1β mRNA (Fig. 1, G and H) and IL-6 mRNA (Fig. S2 C) but had no effect on the decay of NLRP3 mRNA (Fig. 1, I and J). To reinforce these observations, PF-3644022 was used because it directly targets MK2 (Mourey et al., 2010) but not the p38α–MK2 complex. Consistent with the concept of the p38α–MK2 axis, PF-3644022 promoted the degradation of mRNA encoding IL-1β (Fig. 1 K) and TNF-α (Fig. 1 L). The IKK2 inhibitor had no impact on mRNA stability (Fig. 1, G–J), consistent with the function of NF-κB in the regulation of transcription but not posttranscriptional events. Importantly, IL-1β secretion by LPS-primed WT and NOMID BMMs was separately inhibited by both CDD-450 and
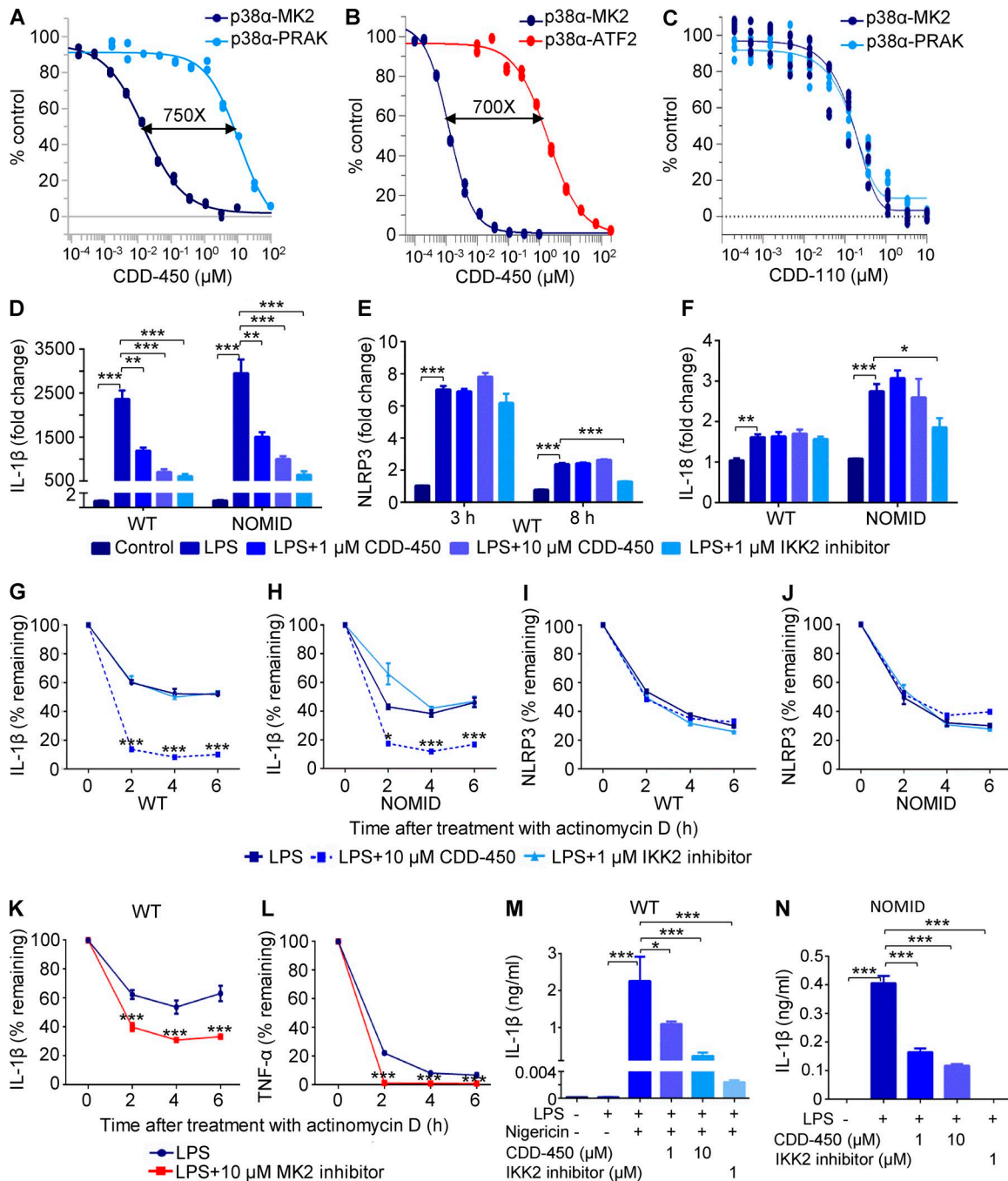
Wang et al.
Inhibition of p38α MAPK–MK2 inhibits inflammation

Journal of Experimental Medicine
https://doi.org/10.1084/jem.20172063

1316

Figure 1. **The selective inhibitor of p38α–MK2, CDD-450, inhibits IL-1β production by promoting IL-1β mRNA instability. (A–C)** Effects of CDD-450 on p38α activation of MK2, PRAK, or ATF2. Activated p38α was added to inactive MK2, inactive PRAK, or ATF2 preincubated with various concentrations of CDD-450 or CDD-110. Phosphorylation of HSP27 peptide (for MK2 or PRAK activity) or ATF2 was determined. **(D–F)** qPCR analysis of IL-1β, NLRP3, and IL-18 mRNA expression. WT and NOMID BMMs were preincubated with CDD-450 or IKK2 inhibitor for 1 h and then with 100 ng/ml LPS for 3 or 8 h. **(G–L)** qPCR analysis of IL-1β, TNF-α, and NLRP3 mRNA stability. BMMs from WT and NOMID mice were stimulated with 100 ng/ml LPS for 3 h and then simultaneously exposed to 1 μg/ml actinomycin D and CDD-450, MK2 inhibitor, or IKK2 inhibitor for 0, 2, 4, or 6 h. **(M and N)** Analysis of IL-1β levels in conditioned media. WT and NOMID BMMs were preincubated with CDD-450 or IKK2 inhibitor for 1 h and then stimulated with 100 ng/ml LPS for 3 h. WT cells were treated for an additional 30 min with 15 μM nigericin. IL-1β levels were measured by ELISA. Data are means ± SEM from experimental triplicates and are representative of at least three independent experiments. *, P < 0.05; **, P < 0.01; ***, P < 0.001.

IKK2 inhibitor (Fig. 1, M and N). Recent evidence implicating kinases in the regulation of the NLRP3 inflammasome (Broz and Dixit, 2016; Man et al., 2017; Song et al., 2017) prompted us to determine the effect of CDD-450 in the activation of this inflammasome, which can be monitored through the binding of the fluorescent FLICA FAM-YVAD-FMK probe to active caspase-1 (Alippe et al., 2017). Exposure of LPS-primed cells to the NLRP3 inflammasome activator nigericin resulted in activation of caspase-1, detected as green fluorescent foci (Fig. S2 D). Concomitant treatment of LPS-stimulated cells with nigericin and

Wang et al.
Inhibition of p38α MAPK–MK2 inhibits inflammation

Journal of Experimental Medicine
https://doi.org/10.1084/jem.20172063

1317

CDD-450 had no effect on this response (Fig. S2 E), which was absent in *caspase-1/11*-deficient cells as expected (Fig. S2 F). Collectively, the results show that CDD-450 inhibits IL-1β production through promotion of IL-1β mRNA instability but not destabilization of inflammasome assembling signals. As a result, this inhibitor should in principle inhibit IL-1β production driven by any inflammasome.

CDD-450 attenuates NOMID-associated complications in mice
NOMID mice were used to evaluate the in vivo role of p38α–MK2 in NOMID pathogenesis. Because constitutive activation of the NLRP3 inflammasome caused premature lethality (Bonar et al., 2012), we generated *Nlrp3*[fl(D301N)/+];*Cre*[ER] mice for postnatal conditional tamoxifen-induced NLRP3 activation and generation of viable adult NOMID mice (conditional NOMID; NOMID[c]). CDD-450 and CDD-111, a global p38α inhibitor previously reported as SD-0006 (Burnette et al., 2009), were formulated in chow with the inhibitor level (parts per million) selected based on achieving sustained >60% inhibition of LPS-induced TNF-α expression (Fig. 2 A). Interestingly, the efficacy of CDD-450 but not CDD-111 in blocking LPS-induced TNF-α expression persisted for up to 4 wk after dosing. These results suggest that the p38α–MK2 specificity exhibited by CDD-450 may avoid transient efficacy associated with global p38α inhibitors. WT mice fed with normal chow or CDD-450 chow gained body weight undistinguishably (Fig. S2 G). In a separate experiment, WT mice fed with CDD-450–containing chow and treated with tamoxifen lost body weight compared with mice given normal chow (Fig. S2 H). Concomitant exposure to CDD-450 chow and tamoxifen was therefore not well tolerated; the underlying mechanisms are unknown. Despite this caveat, CDD-450–treated NOMID[c] mice lost significantly less body weight than untreated NOMID[c] mice (Fig. 2 B). Furthermore, ~35% of untreated NOMID[c] mice developed skin lesions, and 20% of these mice died over the 7-wk period, but neither occurred in CDD-450–treated mice (Fig. 2 C).

Inflammation in NOMID[c] mice was associated with increased p38α phosphorylation (Fig. S2 I), over-production of IL-1β (Fig. 2 D) and IL-18 in bone marrow (Fig. S2 J), and splenomegaly (Fig. 2 E). These responses correlated with an increased number of white blood cells (Fig. 2 F) accompanied by neutrophilia (Fig. 2 G), anemia (Fig. 2 H), thrombocytosis (Fig. 2 I), and inflammation in multiple organs including liver (Fig. 2, J–M, dotted circle), spleen, and brain (not depicted). As shown in these figures, all the inflammatory responses in NOMID mice were attenuated by CDD-450. The antiinflammatory effects of CDD-450 are likely underrepresented because untreated NOMID[c] mice with severe disease died prematurely and were therefore not included in endpoint readouts. Thus, selective inhibition of p38α–MK2 impairs IL-1β and IL-18 secretion and disease manifestations in NOMID[c] mice. CDD-450 likely decreased IL-18 expression in vivo (Fig. S2 J) by indirectly inhibiting systemic inflammation because it had no direct effect on the expression of this cytokine in vitro (Fig. 1 F). Collectively, these findings are consistent with other data indicating that ablation of IL-1 receptor in NOMID mice prevented splenomegaly (Fig. S2 K) and skeletal dysplasia (Wang et al., 2017).

CDD-450 prevents bone destruction in NOMID mice
Skeletal complications including low bone mass are hallmarks of NOMID (Hill et al., 2007). Osteopenia caused by increased osteoclast differentiation was also observed in NOMID mice (Bonar et al., 2012; Snouwaert et al., 2016). An increased number of osteoclasts was observed on trabecular bone surfaces (Fig. 3, A and B, arrowheads) and on cortical bone surfaces (Fig. 3, C and D) in NOMID[c] mice—a phenotype that was prevented by CDD-450. Consistent with in vivo results, CDD-450 inhibited in vitro osteoclast formation induced by RANKL (Fig. 3, E and F), the obligatory osteoclastogenic cytokine that activates p38α among other pathways in osteoclast precursors (Matsumoto et al., 2000; Mansky et al., 2002; Mbalaviele et al., 2006). These results are also consistent with previous research implicating MK2 in physiological and pathological bone resorption through regulation of osteoclast differentiation (Braun et al., 2013). Collectively, these results indicate that treatment with CDD-450 prevents osteopenia in NOMID[c] mice through inhibition of osteoclastogenesis.

CDD-450 inhibits cytokine production in human cells and prevents joint destruction in inflammatory arthritis in rats
To evaluate how these findings may translate into human tissues, experiments were conducted using human peripheral blood monocyte (PBMC) isolated from CAPS patients in which the disease is triggered by exposure to low temperatures and from a healthy control. CAPS PBMC spontaneously produced high amounts of IL-1β at 32°C but not at 37°C (Fig. 4 A), whereas IL-1β production by healthy control PBMC required LPS treatment (Fig. 4 B). In both cases, CDD-450 reduced IL-1β secretion and promoted IL-1β mRNA instability (Fig. 4 C). Although the effects of CDD-450 on NLRP3 and IL-18 mRNA expression in CAPS PBMC were not analyzed, the data show that CDD-450 inhibits IL-1β production by normal and CAPS PBMC.

As noted above, IL-1β production is increased in RA (Mbalaviele et al., 2017). Because IL-1β levels and p38α activity are dysregulated in RA (Mbalaviele and Monahan, 2008) and IL-1β and TNF-α regulate the expression of each other (Bot et al., 1990; Ikejima et al., 1990; Wei et al., 2005; Tian et al., 2013), RA represents another disease for determining the impact of p38α–MK2 inhibition. We found that LPS, TNF-α, and IL-1β robustly stimulated IL-1β, IL-18, and NLRP3 mRNA expression in synovial fibroblasts from an RA patient (Fig. 4, D–F). Because IL-1β was more potent than LPS or TNF-α in regulating its own expression under our experimental conditions, the effects of CDD-450 on IL-1β–induced responses were tested. CDD-450 decreased IL-1β mRNA levels (Fig. 4 G), which correlated with accelerated loss of IL-1β transcripts (Fig. 4 H). In various in vitro systems and animal models, CDD-450 inhibited LPS-induced production of TNF-α and IL-1β with IC_{50} in the 1–10-nM range and IL-6 with IC_{50} in the 100-nM range (Fig. S3, A and B). CDD-450 also accentuated degradation of TNF-α mRNA induced by IL-1β in RA synovial fibroblasts (Fig. 4 I) or LPS in human PBMC (not depicted). Although CDD-450 blocked MK2 phosphorylation induced by IL-1β in RA synovial fibroblasts (Fig. 4 J) and LPS in U937 cells (Fig. S3 C), it had no inhibitory effect on LPS activation of the IKK2, ERK1/2, and JNK pathways in U937 cells (Fig. S3, D–F). It remains unclear whether CDD-450 regulated TNF-α production in vivo directly
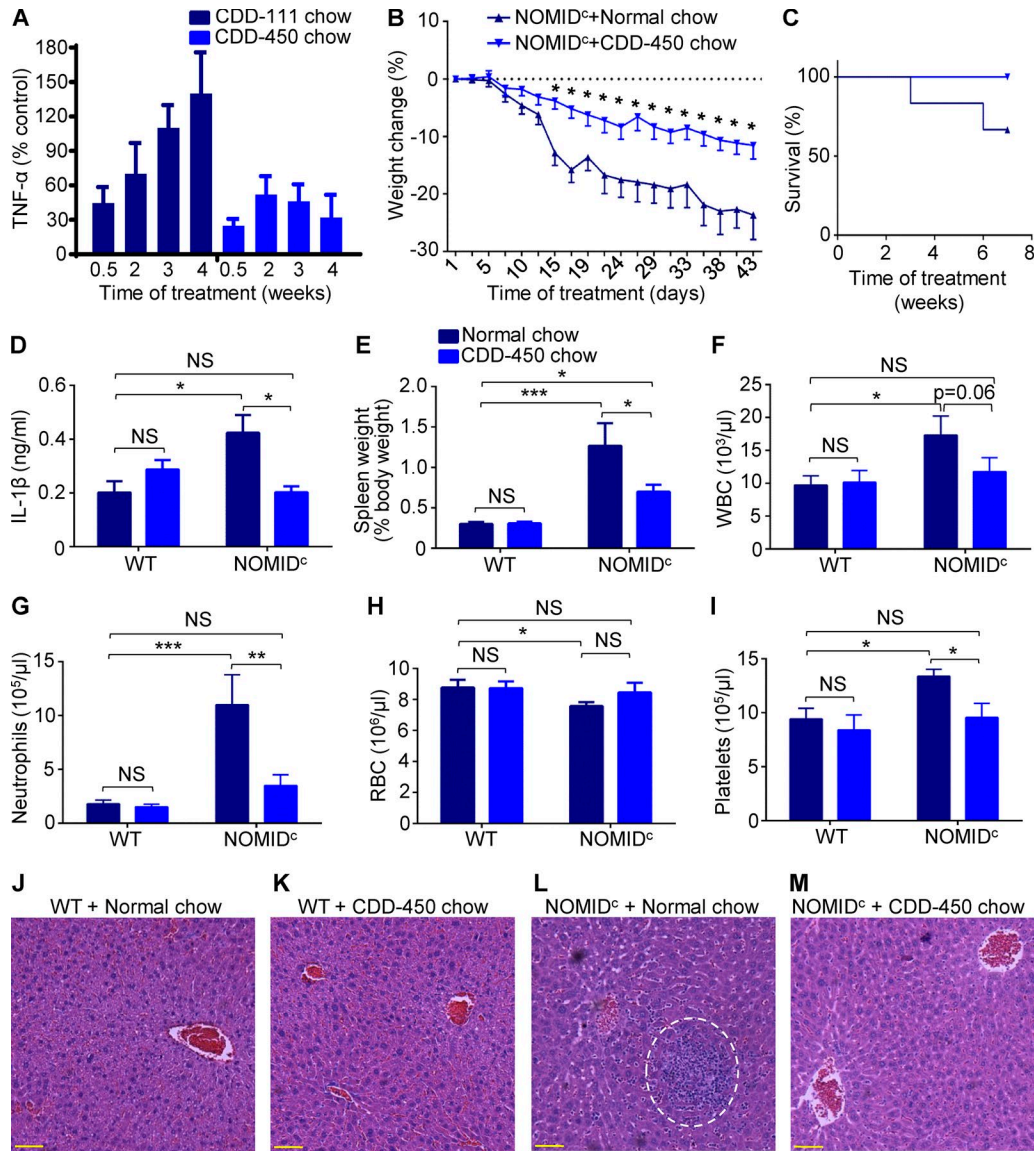
Wang et al.
Inhibition of p38α MAPK–MK2 inhibits inflammation

Journal of Experimental Medicine 1318
https://doi.org/10.1084/jem.20172063

Figure 2. **CDD-450 inhibits inflammatory responses in vivo. (A)** Effects of CDD-450 and CDD-111 on LPS-induced TNF-α production. 8-wk-old WT female mice (six mice/group) were fed with normal chow, CDD-450 (1,000 ppm) chow, or CDD-111 (516 ppm) chow and challenged with LPS (0.025 mg/kg mouse) for 1 h at the indicated time (weeks). TNF-α serum levels were measured by ELISA. **(B and C)** Effects of CDD-450 on body weight and survival. 3-mo-old WT and NOMID[c] littermate mice were fed with normal or CDD-450–formulated chow starting 3 d before sustained tamoxifen administration for 2 wk. Body weight (10–11 mice/group) and survival (12–13 mice/group) was scored every 2–3 d. **(D)** Analysis of IL-1β levels in bone marrow (four to eight mice/group). At the termination of the experiments, bone marrow was harvested and centrifuged, and IL-1β levels in the supernatants were measured by ELISA. **(E)** Spleen weights. **(F–I)** Complete blood counts (four to eight mice/group). Data are means ± SEM. *, P < 0.05; **, P < 0.01; ***, P < 0.001. **(J–M)** H&E staining of liver sections. Dotted circle indicates inflammatory cell infiltrates. Bars, 50 µm. RBC, red blood cell; WBC, white blood cell.

or indirectly via IL-1β. In any case, CDD-450 actions are specific to p38α–MK2 blockade because it spared IKK2, JNK, and ERK1/2 pathways while exhibiting comparable efficacy in inhibiting MK2 and HSP27 phosphorylation and cytokine production.

The efficacy of CDD-450 was evaluated in streptococcal cell wall (SCW)-induced arthritis in the rat, a model in which numerous inflammatory cytokines including TNF-α, IL-6, and IL-1β are highly expressed (Mbalaviele et al., 2006). CDD-450 treatment (oral gavage, 2×/day dosing) was administered therapeutically starting on day 9, the onset period of the chronic inflammatory phase. Arthritis in the SCW model was characterized by the swelling of the hind paw particularly the ankle joints (Fig. 5 A).

CDD-450 inhibited paw swelling as did CDD-110, results that were consistent with 3D microcomputed tomography (µCT) reconstruction pictures showing the joint protective effects of CDD-450 (Fig. 5 B). Bone mineral density was also preserved by CDD-450 (Fig. 5 C). These findings demonstrate that CDD-450 exhibits disease-modifying properties, protecting joints from destruction in a model of inflammatory arthritis.

CDD-450 has the potential to translate the observed preclinical efficacy into clinical studies based upon its oral drug-like properties. Metabolic stability and pharmacokinetic propriety of CDD-450 (e.g., long half-life, low clearance, high oral bioavailability, and high volume of distribution; Fig. S3 G) are consistent
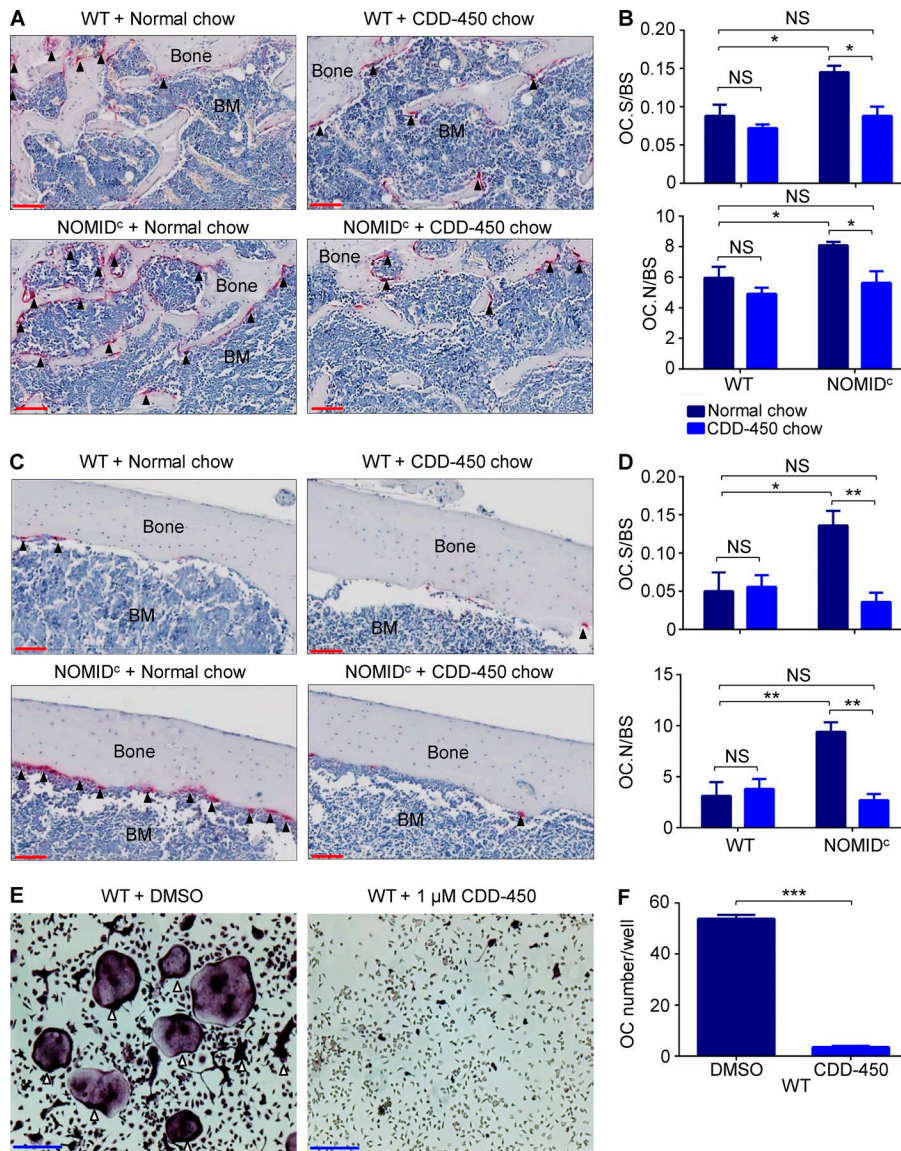
Wang et al.
Inhibition of p38α MAPK–MK2 inhibits inflammation

Journal of Experimental Medicine
https://doi.org/10.1084/jem.20172063

1319

Figure 3. **CDD-450 prevents bone destruction in NOMID[c] mice. (A–F)** 3-mo-old WT and NOMID[c] littermate mice were fed with normal or CDD-450–formulated chow starting 3 d before sustained tamoxifen administration for 2 wk; the experiments were terminated 4 wk later. **(A–D)** Osteoclast (OC) formation in vivo. Bone sections (four to six mice/group) were stained for TRAP activity (red staining). **(A and B)** Osteoclasts (arrowheads) along trabecular bone surfaces were counted. **(C and D)** Osteoclasts along cortical bone surfaces were counted. BM, bone marrow; BS, bone surface; N, number; S, surface. **(E and F)** Effects of CDD-450 on osteoclast formation in vitro. WT BMMs were stimulated with 50 ng/ml RANKL for 4 d in the presence of DMSO (vehicle) or CDD-450. Cultures were stained for TRAP activity, and the number of osteoclasts was determined by counting TRAP+-multinucleated cells with at least three nuclei (arrowheads). In vivo data are means ± SEM; in vitro data are means ± SEM from experimental triplicates and are representative of at least three independent experiments. *, P < 0.05; **, P < 0.01; ***, P < 0.001. Bars, 100 µm.

with oral, 1×/day or 2×/day dosing in humans. Furthermore, CDD-450 was not genotoxic or mutagenic and did not inhibit the cardiac hERG channel. In vivo safety experiments in the rat suggest that CDD-450 was well tolerated at exposures >30× higher than the predicted Cmax efficacious exposure (Fig. S3 G).

In conclusion, CDD-450 selectively blocks p38α activation of the proinflammatory kinase MK2 while sparing p38α activation of other effectors such as PRAK and ATF2. Use of CDD-450 helped to reveal a critical role of the p38α–MK2 pathway in NLRP3 inflammasome priming. CDD-450 also inhibited other inflammatory pathways (e.g., TNF-α and IL-6), implying that potential indications for this drug candidate expand beyond inflammasopathies. These findings may have clinical implications because CDD-450 (a) is at least as efficacious as clinically evaluated global p38α inhibitors in suppressing inflammation in both animal disease models and patients' cells, and (b) it offers the potential to avoid transient efficacy associated with global p38 inhibitors that may result from their inhibition of non-MK2 substrates involved in antiinflammatory and housekeeping functions.

Materials and methods
Animals and inhibitors

Cre-ER[TM] (B6.Cg-Tg(CAG-cre/Esr1*)5Amc/J) mice and IL-1 receptor–deficient (*Il-1r^{−/−}*) mice were purchased from The Jackson Laboratory. *Nlrp3[fl(D301N)/+]* mice have been previously described (Bonar et al., 2012; Wang et al., 2017). *Cre-ER[TM]* mice and *Nlrp3[fl(D301N)/+]* mice were crossed to generate *Nlrp3[fl(D301N)/+]*; *Cre-ER[TM]* mice and *Cre-ER[TM]* mice. Injection of tamoxifen (i.p.; 75 mg/kg body weight; Sigma-Aldrich) once every other day, three times per week for 2 wk to *Nlrp3[fl(D301N)/+]*;*Cre-ER[TM]* mice and *Cre-ER[TM]* mice yielded NOMID[c] mice and control mice, respectively. NOMID mice with constitutive activation of NLRP3 in myeloid cells driven by *lysozyme M-Cre* have been previously described (Wang et al., 2017). *Caspase-1/11*–deficient mice were purchased from The Jackson Laboratory. All mice were on the C57BL/6 background for >10 generations, and mouse genotyping was performed by PCR. SCW arthritis in rats was induced as previously described (Mbalaviele et al., 2006). In brief, adult female Lewis rats (180 g) were injected i.p. with 15 mg/kg, body weight, of the SCW preparation (BD). The acute
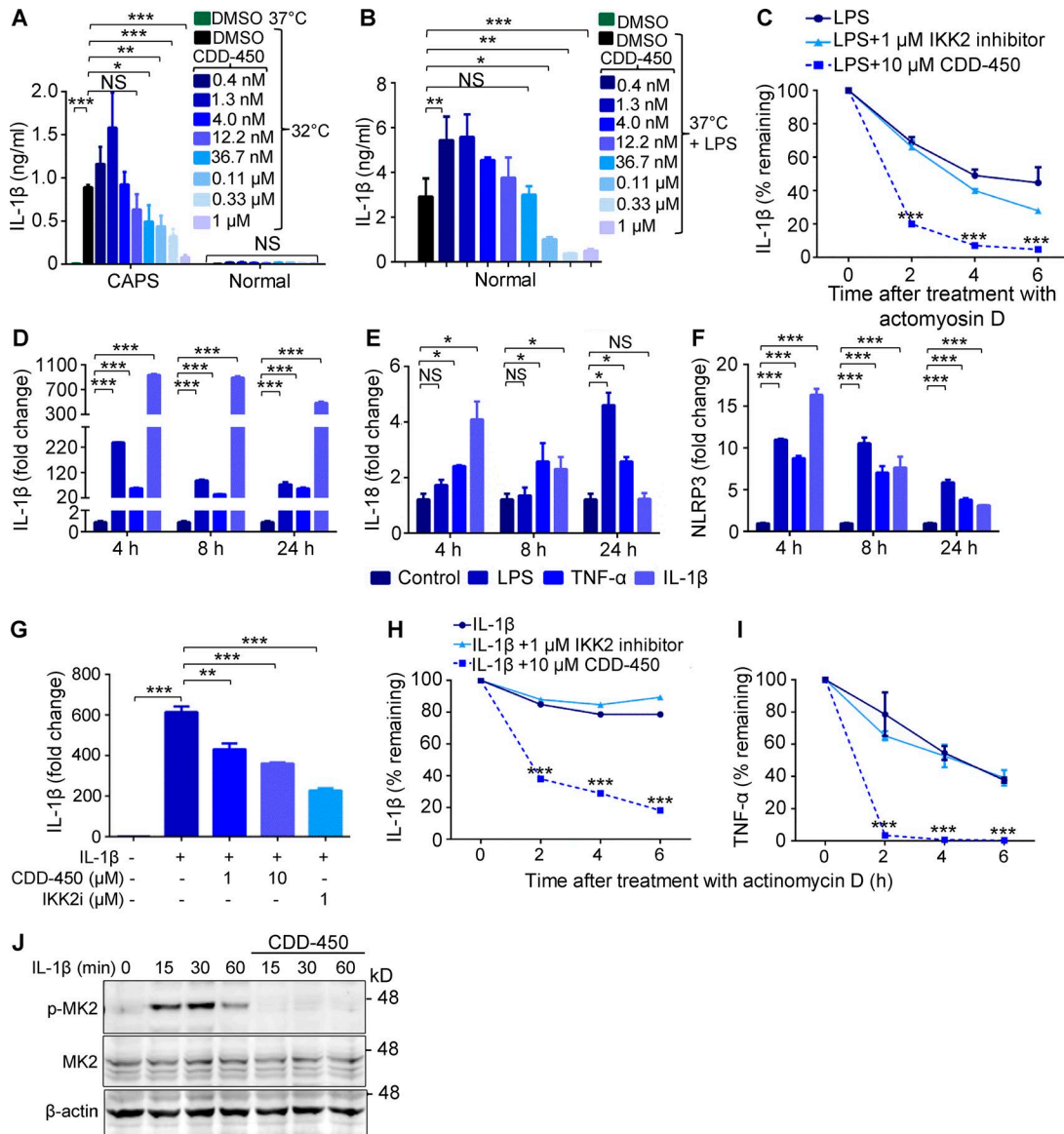
Figure 4. **CDD-450 inhibits cytokine production in human cells. (A)** Effects of CDD-450 on IL-1β production by PBMC isolated from CAPS patients or healthy controls. Cells were cultured for 16 h at 32°C or 37°C in the presence of DMSO or CDD-450. IL-1β levels in conditioned media were determined by ELISA. **(B)** Effects of CDD-450 on LPS-stimulated IL-1β production by normal human PBMC. Cells were stimulated with 100 ng/ml LPS for 16 h at 37°C in the presence of DMSO or CDD-450. **(C)** qPCR analysis of the effects of CDD-450 or IKK2 inhibitor on IL-1β mRNA stability in normal human PBMC. Cells were stimulated with 10 ng/ml LPS for 3 h and then simultaneously exposed to 1 µg/ml actinomycin D and CDD-450 or IKK2 inhibitor. **(D–F)** qPCR analysis of the effects of LPS (100 ng/ml), TNF-α (10 ng/ml), or IL-1β (10 ng/ml) on IL-1β, IL-18, and NLRP3 mRNA expression by synovial fibroblasts from an RA patient. **(G)** qPCR analysis of the effects of CDD-450 or IKK2 inhibitor on IL-1β mRNA expression by synovial fibroblasts from RA patient. Cells were preincubated with the inhibitors for 1 h before treatment with 10 ng/ml IL-1β for 3 h. **(H and I)** qPCR analysis of the effects of CDD-450 or IKK2 inhibitor on IL-1β and TNF-α mRNA stability in synovial fibroblasts from an RA patient. Cells were stimulated with 10 ng/ml IL-1β for 3 h and then simultaneously exposed to 1 µg/ml actinomycin D and CDD-450 or IKK2 inhibitor. Data are means ± SEM from experimental triplicates and are representative of at least two independent experiments. *, $P < 0.05$; **, $P < 0.01$; ***, $P < 0.001$. **(J)** Effect of CDD-450 on MK2 phosphorylation induced by IL-1β. Synovial fibroblasts were preincubated with 10 µM CDD-450 for 1 h and then treated with 10 ng/ml IL-1β. Samples were analyzed by Western blotting.

phase of the disease was monitored by measuring paw edema between days 2 and 8. On day 9, rats displaying paw edema were sorted into groups (8 rats/group) and then dosed with the inhibitors by oral gavage. Edema was monitored by measuring paw volume using a plethysmometer every other day until day 21. All procedures were approved by the Institutional Animal Care and Use Committee of Washington University School of Medicine in St. Louis. CDD-450 is a proprietary inhibitor of

Aclaris Therapeutics Inc. The IKK2 and MK2 inhibitors used in this study were reported as PHA-408 (Mbalaviele et al., 2009) and PF-3644022 (Mourey et al., 2010), respectively, whereas the two global p38 inhibitors used, CDD-111 and CDD-110, were reported as SD-0006 (Burnette et al., 2009) and PH-797804 (Hope et al., 2009), respectively. CDD-110 was the racemate of PH-797804. All of these compounds were synthesized by Confluence Discovery Technologies, Inc.
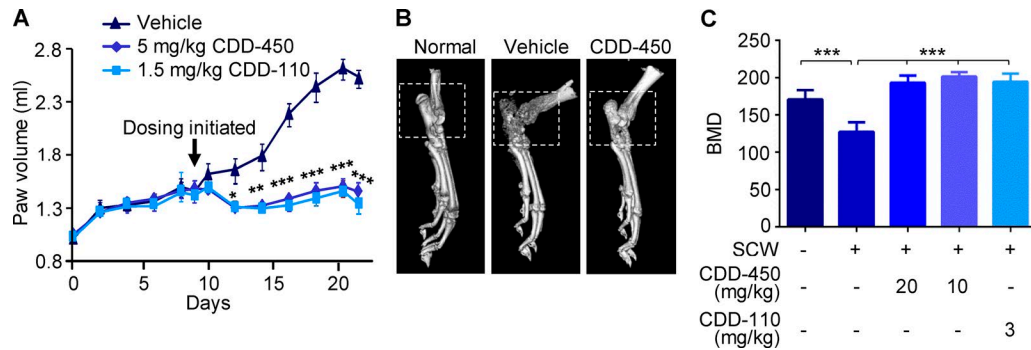
Wang et al.
Inhibition of p38α MAPK–MK2 inhibits inflammation

Journal of Experimental Medicine
https://doi.org/10.1084/jem.20172063

1321

Figure 5. **CDD-450 prevents joint destruction in inflammatory arthritis in rats. (A–C)** Effects of CDD-450 or CDD-110 on paw swelling and bone destruction in SCW-induced arthritis. SCW preparations were injected into rats i.p. On day 9, rats displaying paw edema were sorted into groups (eight rats/group) and dosed daily with vehicle, 5, or 10 mg/kg CDD-450 2×/day (10 mg/kg/d or 20 mg/kg/d, respectively) or 1.5 mg/kg CDD-110 2×/day (3 mg/kg/d). **(A)** Paw volume measurements. **(B)** 3D μCT reconstruction of paws from rats treated with 5 mg/kg CDD-450 2×/day (10 mg/kg/d). **(C)** Bone mineral density (BMD) measurements corresponding with the area delineated by the dashed squares in B. Data are means ± SEM. *, P < 0.05; **, P < 0.01; ***, P < 0.001.

LPS endotoxemia

Adult male Lewis rats (200–220 g; five/group; Harlan Sprague Dawley) and adult female mice (18–20 g; Charles River Labs) were fasted for 18 h before oral dosing. Compounds were prepared as fine aqueous suspensions in 0.5% methylcelluose and 0.025% Tween-20 in PBS (Sigma-Aldrich) and administered by oral gavage in a volume of 0.5 ml for 1 h before intravenous injection of LPS (*Escherichia coli* serotype 0111:B4 for rats or *Salmonella typhosa* for mice; Sigma-Aldrich) at a dose of 1 mg/kg (rats) or 0.025 mg/kg (mice) in 0.5 ml sterile saline (Baxter Healthcare). Blood was collected in serum separator tubes via cardiac puncture 90 min (rats) or 60 min (mice) after LPS injection. Serum was stored at –20°C until TNF-α levels were determined using a Proinflammatory Panel 1 mouse kit (Meso-Scale Diagnostics).

For IL-1β and IL-18 measurements in bone marrow, flushed bone marrow was centrifuged, and the supernatants were collected as described previously (Bonar et al., 2012). IL-1β and IL-18 levels were quantified using the eBioscience ELISA kit and Meso-Scale Diagnostics kit, respectively.

Peripheral blood analyses

Complete blood counts were performed by the Washington University School of Medicine Division of Comparative Medicine Diagnostic Laboratory as previously described (Wang et al., 2017).

Cell cultures

For all in vitro pharmacology experiments except otherwise specified, cells were pretreated with vehicle (0.5% DMSO, final concentration) or inhibitors (in 0.5% DMSO, final concentration) for 1 h before stimulation with the indicated ligand or ligands. Protein expression or phosphorylation was measured by ELISA, Western blotting, or using MesoScale Diagnostics kits.

BMMs were obtained by culturing mouse bone marrow cells in culture media containing a 1:10 dilution of supernatant from the fibroblastic cell line CMG 14-12 as a source of macrophage colony–stimulating factor (Takeshita et al., 2000), a mitogenic factor for BMMs, for ~5 d in a 10-cm dish as previously described

(Alippe et al., 2017). Nonadherent cells were removed by vigorous washes with PBS, and adherent BMMs were detached with trypsin-EDTA and cultured in culture media containing a 1:10 dilution of supernatant from the fibroblastic cell line CMG 14-12.

To activate the NLRP3 inflammasome, BMMs were plated at 10^4 cells per well on a 96-well plate and maintained for 24 h in culture media containing a 1:10 dilution of CMG supernatant. Cells were pretreated with vehicle, CDD-450, or IKK2 inhibitor, followed by treatment with 100 ng/ml LPS or PBS without changing media for 3 h and then with 15 μM nigericin (AdipoGen) for 30 min, and conditioned media were collected for IL-1β analysis.

For osteoclast formation, BMM were plated at $5 × 10^3$ cells per well in a 96-well plate in culture media containing a 1:50 dilution of CMG and 100 ng/ml receptor activator of NF-κB ligand (RANKL), a required cytokine for osteoclast differentiation. Media with supplements were changed every other day and maintained at 37°C in a humidified atmosphere of 5% CO_2 in air.

Synovial fibroblasts from RA tissues were obtained as previously described (Mbalaviele et al., 2009). Human PBMCs were isolated from a CAPS patient or healthy control following procedures approved by Ethics Committees of the University of California, San Diego, and Washington University School of Medicine in St. Louis.

Human whole blood obtained from healthy human volunteers was preincubated with vehicle or various concentrations of CDD-450 before treatment with 100 ng/ml LPS (Sigma-Aldrich) for 4 h at 37°C with 5% CO_2. Samples were centrifuged at 1,800 g for 5 min, and then supernatants were harvested and assayed for TNF-α production.

Rat whole blood was collected by cardiac puncture into heparin vacutainer tubes and centrifuged to obtain plasma, which was used to measure TNF-α levels.

Human premonocytic cells (U937; ATCC) grown in RPMI 1640 containing 10% FBS (Gibco) were induced to differentiate into macrophages upon treatment with 20 ng/ml PMA (Sigma-Aldrich) for 24 h. Cells were then pretreated with vehicle or CDD-450 before stimulation with 100 ng/ml LPS (Sigma-Aldrich) for 4 h. TNF-α, IL-1β, and IL-6 levels were measured in conditioned media.

Wang et al.
Inhibition of p38α MAPK–MK2 inhibits inflammation

Journal of Experimental Medicine
https://doi.org/10.1084/jem.20172063

1322

Histology

Tissue samples were processed as described previously (Wang et al., 2017). In brief, long bones were fixed in 10% formalin, decalcified in 14% (wt/vol) EDTA, pH 7.2, for 10–14 d at room temperature, embedded in paraffin, sectioned at 5-µm thicknesses, and mounted on glass slides. The sections were stained with H&E and tartrate-resistant acidic phosphatase (TRAP) as described previously (Wang et al., 2017). Photographs were taken using NanoZoomer (Hamamatsu Photonics).

Bone mass and microstructure

Hind paws obtained from Lewis female rats were analyzed at day 21 by µCT system (vivaCT 40; Scanco Medical AG) as previously described (Mbalaviele et al., 2006).

TRAP staining

Cytochemical staining for TRAP was used to identify osteoclasts as described previously (Alippe et al., 2017). In brief, cells on a 96-well plate were fixed with 3.7% formaldehyde and 0.1% Triton X-100 for 10 min at room temperature. The cells were rinsed with water and incubated with the TRAP staining solution (leukocyte acid phosphatase kit; Sigma-Aldrich) at room temperature for 30 min. Under light microscopy, multinuclear TRAP-positive cells with ≥3 nuclei were scored as osteoclasts.

mRNA expression analysis

Total RNA was harvested from cultured cells using the PureLink RNA mini kit (Invitrogen). Complementary DNA was then synthesized with the iScript reverse transcription kit (Bio-Rad Laboratories) and quantified using primers listed in Table S1. Gene expression was analyzed by quantitative PCR (qPCR) using the SYBR green gene expression assay (Applied Biosystems). To study mRNA stability, cells were treated with PBS, 100 ng/ml LPS, or 10 ng/ml IL-1β for 3 h and then exposed to 1 µg/ml actinomycin D (Sigma-Aldrich) to block RNA synthesis and/or CDD-450, IKK2 inhibitor, or MK2 inhibitor, and cells were lysed 0, 2, 4, or 6 h later. Total RNA was extracted, and then the rates of IL-1β, IL-6, NLRP3, and TNF-α mRNA decay were monitored by qPCR.

Western blot analysis

Cell extracts were prepared by lysing cells with RIPA buffer (50 mM Tris, 150 mM NaCl, 1 mM EDTA, 0.5% NaDOAc, 0.1% SDS, and 1.0% NP-40) plus phosphatase and protease inhibitors (2 mM $NaVO_4$, 10 mM NaF, and 1 mM PMSF) and cOmplete protease inhibitor cocktail (Roche). For tissue extracts, liver tissues were homogenized and lysed with RIPA buffer containing phosphatase and protease inhibitors. Protein concentrations were determined by the Bio-Rad Laboratories method, and equal amounts of proteins were subjected to SDS-PAGE gels (12%). Proteins were transferred onto nitrocellulose membranes and incubated with p-MK2 (Thr334), MK2, p-p38α, p38α antibody (1:1,000; Cell Signaling Technologies), NLRP3 antibody (AdipoGen), pro–caspase-1, or β-actin antibody (Santa Cruz Biotechnology, Inc.) overnight at 4°C followed by incubation for 1 h with secondary goat anti–mouse IRDye 800 (Rockland) or goat anti–rabbit Alexa Fluor 680 (Molecular Probes), respectively. The results were visualized using the Odyssey infrared imaging system (LI-COR Biosciences).

Microscopic analysis of active caspase-1

BMM were plated at 5×10^4 cells per well on a 96-well plate and maintained for 24 h in culture media. They were primed with 100 ng/ml LPS for 3 h and treated with 10 µM CDD-450 and/or 15 µM nigericin for 30 min. Cells were incubated with the FLICA FAM-YVAD-FMK probe (ImmunoChemistry Technologies) for 30 min at 37°C, washed twice with PBS/FBS, and fixed with 10% buffered formalin. Cells were then counterstained with Fluoro gel II containing DAPI (Electron Microscopy Sciences). Images were taken with a DP70 Olympus digital camera coupled with an IX51 Olympus inverted microscope, captured with QCapture Pro software (QImaging), and analyzed with ImageJ software (National Institutes of Health).

p38α–MK2, p38α–PRAK, and p38α–ATF2 assays

Inactive p38α (2 µM) was incubated with MgATP (200 µM) and constitutively active MKK6 (40 nM) in buffer containing 25 mM Hepes, pH 7.6, 10 mM $MgCl_2$, 0.01% Triton X-100, 0.01% BSA, and 1 mM DTT for 2 h at room temperature. p38α activity (60 pM, final concentration) toward nonphosphorylated GST-MK2 (1 nM, final concentration) or nonphosphorylated GST-PRAK (10 nM, final concentration) was determined by measuring MK2 or PRAK kinase activity via phosphorylation of a fluorescently labeled HSP27 peptide (FITC KKKALSRQLSVAA). HSP27 peptide substrate and MgATP were held constant at 1 µM and 10 µM, respectively. HSP27 phosphorylation was quantified using IMAP assay technology (Molecular Devices) and the Analyst HT plate reader (Surplus Solutions LLC) using standard fluorescence polarization settings. ATF2 and MgATP were held constant at 100 nM and 4 µM, respectively, and incubated with p38α (62.5 pM, final concentration) at room temperature to measure ATF2 phosphorylation. Phosphorylated ATF2 was measured using the MesoScale Diagnostics kit. Inhibitor potency was calculated by fitting dose–response data to the four-parameter logistical IC_{50} equation.

Surface plasmon resonance analysis

All reactions were performed at room temperature. The CM5 sensor chip was prepared using standard Biacore methodology. In brief, after docking and priming with distilled water using the QUICKINJECT command, the CM5 surface was subjected to two consecutive 20-µl pulses each of 50 mM NaOH, 10 mM HCl, 0.1% SDS, and 0.085% H_3PO_4 at a flow of 100 µl/min. Afterward, the integrated microfluidic cartridge was washed and primed with running buffer. To activate the CM5 surface, 400 mM 1-ethyl-3-(3-dimethylaminopropyl) carbodiimide hydrochloride and 100 mM N-hydroxysuccinimide (GE Healthcare) were mixed 50:50, and the mixture was injected for 7 min (35 µl) at a flow rate of 5 µl/min. Next, the anti-GST antibody (GE Healthcare) was diluted in 10 mM NaOAc and injected over the desired flow cell. This was then followed by a 7-min (35 µl) injection of ethanolamine. For amine coupling and testing of inhibitors, the running buffer consisted of 10 mM Hepes, 150 mM NaCl, 1 mM Tris (2-carboxyethyl) phosphine HCl, and 0.005% Tween-20. The running buffer was filtered (0.45 µm) and degassed at 25°C before use.

GST-MK2 (EMD Millipore) was captured with the amine-coupled anti-GST antibody for 2 min. Afterward, recombinant p38α (10 nM; Invitrogen) was injected in the presence or absence of

CDD-450 or CDD-110 at a flow rate of 30 μl/min. The binding was evaluated using Biacore 2000, and raw sensorgram data were processed using BiaEvaluation (3.1; GE Healthcare).

Kinase selectivity

Selectivity experiments were performed at Thermo Fisher Scientific.

Statistical analysis

Statistical analysis was performed using the Student's t test, one-way ANOVA with Tukey's multiple comparisons test, or two-way ANOVA with Sidak's multiple comparisons test as well as the Log-rank (Mantel-Cox) test for comparison of survival curves in Prism (6.0; GraphPad Software).

Online supplemental material

Fig. S1 shows binding and selectivity properties of CDD-450. Fig. S2 shows the effects of inhibitors and deletion of IL-1 receptors on p38α–MK2 signaling, IL-1β and TNF-α mRNA stability, and inflammation. Fig. S3 shows the properties of CDD-450 and its effects on IL-1β, IL-6, and TNF-α production. Table S1 shows the list of primers used for qPCR analyses.

References

Agostini, L., F. Martinon, K. Burns, M.F. McDermott, P.N. Hawkins, and J. Tschopp. 2004. NALP3 forms an IL-1beta-processing inflammasome with increased activity in Muckle-Wells autoinflammatory disorder. *Immunity.* 20:319–325. https://doi.org/10.1016/S1074-7613(04)00046-9

Alippe, Y., C. Wang, B. Ricci, J. Xiao, C. Qu, W. Zou, D.V. Novack, Y. Abu-Amer, R. Civitelli, and G. Mbalaviele. 2017. Bone matrix components activate the NLRP3 inflammasome and promote osteoclast differentiation. *Sci. Rep.* 7:6630. https://doi.org/10.1038/s41598-017-07014-0

Bauernfeind, F.G., G. Horvath, A. Stutz, E.S. Alnemri, K. MacDonald, D. Speert, T. Fernandes-Alnemri, J. Wu, B.G. Monks, K.A. Fitzgerald, et al. 2009. Cutting edge: NF-kappaB activating pattern recognition and cytokine receptors license NLRP3 inflammasome activation by regulating NLRP3 expression. *J. Immunol.* 183:787–791. https://doi.org/10.4049/jimmunol.0901363

Bonar, S.L., S.D. Brydges, J.L. Mueller, M.D. McGeough, C. Pena, D. Chen, S.K. Grimston, C.L. Hickman-Brecks, S. Ravindran, A. McAlinden, et al. 2012. Constitutively activated NLRP3 inflammasome causes inflammation and abnormal skeletal development in mice. *PLoS One.* 7:e35979. https://doi.org/10.1371/journal.pone.0035979

Bot, F.J., P. Schipper, L. Broeders, R. Delwel, K. Kaushansky, and B. Löwenberg. 1990. Interleukin-1 alpha also induces granulocyte-macrophage colony-stimulating factor in immature normal bone marrow cells. *Blood.* 76:307–311.

Braun, T., J. Lepper, G. Ruiz Heiland, W. Hofstetter, M. Siegrist, P. Lezuo, M. Gaestel, M. Rumpler, R. Thaler, K. Klaushofer, et al. 2013. Mitogen-activated protein kinase 2 regulates physiological and pathological bone turnover. *J. Bone Miner. Res.* 28:936–947. https://doi.org/10.1002/jbmr.1816

Broz, P., and V.M. Dixit. 2016. Inflammasomes: mechanism of assembly, regulation and signalling. *Nat. Rev. Immunol.* 16:407–420. https://doi.org/10.1038/nri.2016.58

Burnette, B.L., S. Selness, R. Devraj, G. Jungbluth, R. Kurumbail, L. Stillwell, G. Anderson, S. Mnich, J. Hirsch, R. Compton, et al. 2009. SD0006: a potent, selective and orally available inhibitor of p38 kinase. *Pharmacology.* 84:42–60. https://doi.org/10.1159/000227286

Cumming, J.G., J.E. Debreczeni, F. Edfeldt, E. Evertsson, M. Harrison, G.A. Holdgate, M.J. James, S.G. Lamont, K. Oldham, J.E. Sullivan, and S.L. Wells. 2015. Discovery and characterization of MAPK-activated protein kinase-2 prevention of activation inhibitors. *J. Med. Chem.* 58:278–293. https://doi.org/10.1021/jm501038s

de Jesus, A.A., S.W. Canna, Y. Liu, and R. Goldbach-Mansky. 2015. Molecular mechanisms in genetically defined autoinflammatory diseases: disorders of amplified danger signaling. *Annu. Rev. Immunol.* 33:823–874. https://doi.org/10.1146/annurev-immunol-032414-112227

Genovese, M.C., S.B. Cohen, D. Wofsy, M.E. Weinblatt, G.S. Firestein, E. Brahn, V. Strand, D.G. Baker, and S.E. Tong. 2011. A 24-week, randomized, double-blind, placebo-controlled, parallel group study of the efficacy of oral SCIO-469, a p38 mitogen-activated protein kinase inhibitor, in patients with active rheumatoid arthritis. *J. Rheumatol.* 38:846–854. https://doi.org/10.3899/jrheum.100602

Hale, Karen K., David Trollinger, Marynette Rihanek, and Carl L. Manthey. 1999. Differential Expression and Activation of p38 Mitogen-Activated Protein Kinase α, β, γ, and δ in Inflammatory Cell Lineages. *J. Immunol.* 162:4246–4252.

Hammaker, D., and G.S. Firestein. 2010. "Go upstream, young man": lessons learned from the p38 saga. *Ann. Rheum. Dis.* 69(Suppl 1):i77–i82. https://doi.org/10.1136/ard.2009.119479

Hegen, M., M. Gaestel, C.L. Nickerson-Nutter, L.L. Lin, and J.B. Telliez. 2006. MAPKAP kinase 2-deficient mice are resistant to collagen-induced arthritis. *J. Immunol.* 177:1913–1917. https://doi.org/10.4049/jimmunol.177.3.1913

Hill, S.C., M. Namde, A. Dwyer, A. Poznanski, S. Canna, and R. Goldbach-Mansky. 2007. Arthropathy of neonatal onset multisystem inflammatory disease (NOMID/CINCA). *Pediatr. Radiol.* 37:145–152. https://doi.org/10.1007/s00247-006-0358-0

Hitti, E., T. Iakovleva, M. Brook, S. Deppenmeier, A.D. Gruber, D. Radzioch, A.R. Clark, P.J. Blackshear, A. Kotlyarov, and M. Gaestel. 2006. Mitogen-activated protein kinase-activated protein kinase 2 regulates tumor necrosis factor mRNA stability and translation mainly by altering tristetraprolin expression, stability, and binding to adenine/uridine-rich element. *Mol. Cell. Biol.* 26:2399–2407. https://doi.org/10.1128/MCB.26.6.2399-2407.2006

Hoffman, H.M., and L. Broderick. 2016. The role of the inflammasome in patients with autoinflammatory diseases. *J. Allergy Clin. Immunol.* 138:3–14. https://doi.org/10.1016/j.jaci.2016.05.001

Hoffman, H.M., and S.D. Brydges. 2011. Genetic and molecular basis of inflammasome-mediated disease. *J. Biol. Chem.* 286:10889–10896. https://doi.org/10.1074/jbc.R110.135491

Hope, H.R., G.D. Anderson, B.L. Burnette, R.P. Compton, R.V. Devraj, J.L. Hirsch, R.H. Keith, X. Li, G. Mbalaviele, D.M. Messing, et al. 2009. Anti-inflammatory properties of a novel N-phenyl pyridinone inhibitor of p38 mitogen-activated protein kinase: preclinical-to-clinical translation. *J. Pharmacol. Exp. Ther.* 331:882–895. https://doi.org/10.1124/jpet.109.158329

Ikejima, T., S. Okusawa, P. Ghezzi, J.W. van der Meer, and C.A. Dinarello. 1990. Interleukin-1 induces tumor necrosis factor (TNF) in human peripheral blood mononuclear cells in vitro and a circulating TNF-like activity in rabbits. *J. Infect. Dis.* 162:215–223. https://doi.org/10.1093/infdis/162.1.215

Kolly, L., N. Busso, G. Palmer, D. Talabot-Ayer, V. Chobaz, and A. So. 2010. Expression and function of the NALP3 inflammasome in rheumatoid synovium. *Immunology.* 129:178–185. https://doi.org/10.1111/j.1365-2567.2009.03174.x

Koné-Paut, I., and C. Galeotti. 2015. Current treatment recommendations and considerations for cryopyrin-associated periodic syndrome. *Expert Rev. Clin. Immunol.* 11:1083–1092. https://doi.org/10.1586/1744666X.2015.1077702

Korb, A., M. Tohidast-Akrad, E. Cetin, R. Axmann, J. Smolen, and G. Schett. 2006. Differential tissue expression and activation of p38 MAPK alpha, beta, gamma, and delta isoforms in rheumatoid arthritis. *Arthritis Rheum.* 54:2745–2756. https://doi.org/10.1002/art.22080

Kotlyarov, A., A. Neininger, C. Schubert, R. Eckert, C. Birchmeier, H.D. Volk, and M. Gaestel. 1999. MAPKAP kinase 2 is essential for LPS-induced TNF-alpha biosynthesis. *Nat. Cell Biol.* 1:94–97. https://doi.org/10.1038/10061

Kyttaris, V.C. 2012. Kinase inhibitors: a new class of antirheumatic drugs. *Drug Des. Devel. Ther.* 6:245–250. https://doi.org/10.2147/DDDT.S25426

Man, S.M., R. Karki, and T.D. Kanneganti. 2017. Molecular mechanisms and functions of pyroptosis, inflammatory caspases and inflammasomes in infectious diseases. *Immunol. Rev.* 277:61–75. https://doi.org/10.1111/imr.12534

Mansky, K.C., U. Sankar, J. Han, and M.C. Ostrowski. 2002. Microphthalmia transcription factor is a target of the p38 MAPK pathway in response to receptor activator of NF-kappa B ligand signaling. *J. Biol. Chem.* 277:11077–11083. https://doi.org/10.1074/jbc.M111696200

Matsumoto, M., T. Sudo, T. Saito, H. Osada, and M. Tsujimoto. 2000. Involvement of p38 mitogen-activated protein kinase signaling pathway in osteoclastogenesis mediated by receptor activator of NF-kappa B ligand (RANKL). *J. Biol. Chem.* 275:31155–31161. https://doi.org/10.1074/jbc.M001229200

Mayor, F. Jr., M. Jurado-Pueyo, P.M. Campos, and C. Murga. 2007. Interfering with MAP kinase docking interactions: implications and perspective for the p38 route. *Cell Cycle.* 6:528–533. https://doi.org/10.4161/cc.6.5.3920

Mbalaviele, G., and J.B. Monahan. 2008. Mechanisms of the joint-protective effects of p38 MAPK inhibitors in rodent arthritis. *Expert Opin. Drug Discov.* 3:163–172. https://doi.org/10.1517/17460441.3.2.163

Mbalaviele, G., G. Anderson, A. Jones, P. De Ciechi, S. Settle, S. Mnich, M. Thiede, Y. Abu-Amer, J. Portanova, and J. Monahan. 2006. Inhibition of p38 mitogen-activated protein kinase prevents inflammatory bone destruction. *J. Pharmacol. Exp. Ther.* 317:1044–1053. https://doi.org/10.1124/jpet.105.100362

Mbalaviele, G., C.D. Sommers, S.L. Bonar, S. Mathialagan, J.F. Schindler, J.A. Guzova, A.F. Shaffer, M.A. Melton, L.J. Christine, C.S. Tripp, et al. 2009. A novel, highly selective, tight binding IkappaB kinase-2 (IKK-2) inhibitor: a tool to correlate IKK-2 activity to the fate and functions of the components of the nuclear factor-kappaB pathway in arthritis-relevant cells and animal models. *J. Pharmacol. Exp. Ther.* 329:14–25. https://doi.org/10.1124/jpet.108.143800

Mbalaviele, G., D.V. Novack, G. Schett, and S.L. Teitelbaum. 2017. Inflammatory osteolysis: a conspiracy against bone. *J. Clin. Invest.* 127:2030–2039. https://doi.org/10.1172/JCI93356

McGeough, M.D., A. Wree, M.E. Inzaugarat, A. Haimovich, C.D. Johnson, C.A. Peña, R. Goldbach-Mansky, L. Broderick, A.E. Feldstein, and H.M. Hoffman. 2017. TNF regulates transcription of NLRP3 inflammasome components and inflammatory molecules in cryopyrinopathies. *J. Clin. Invest.*

Mourey, R.J., B.L. Burnette, S.J. Brustkern, J.S. Daniels, J.L. Hirsch, W.F. Hood, M.J. Meyers, S.J. Mnich, B.S. Pierce, M.J. Saabye, et al. 2010. A benzothiophene inhibitor of mitogen-activated protein kinase-activated protein kinase 2 inhibits tumor necrosis factor alpha production and has oral anti-inflammatory efficacy in acute and chronic models of inflammation. *J. Pharmacol. Exp. Ther.* 333:797–807. https://doi.org/10.1124/jpet.110.166173

Neven, B., I. Marvillet, C. Terrada, A. Ferster, N. Boddaert, V. Couloignier, G. Pinto, A. Pagnier, C. Bodemer, B. Bodaghi, et al. 2010. Long-term efficacy of the interleukin-1 receptor antagonist anakinra in ten patients with neonatal-onset multisystem inflammatory disease/chronic infantile neurologic, cutaneous, articular syndrome. *Arthritis Rheum.* 62:258–267. https://doi.org/10.1002/art.25057

Qu, C., S.L. Bonar, C.L. Hickman-Brecks, S. Abu-Amer, M.D. McGeough, C.A. Peña, L. Broderick, C. Yang, S.K. Grimston, J. Kading, et al. 2015. NLRP3 mediates osteolysis through inflammation-dependent and -independent mechanisms. *FASEB J.* 29:1269–1279. https://doi.org/10.1096/fj.14-264804

Rigante, D., A. Leone, R. Marrocco, M.E. Laino, and A. Stabile. 2011. Long-term response after 6-year treatment with anakinra and onset of focal bone erosion in neonatal-onset multisystem inflammatory disease (NOMID/CINCA). *Rheumatol. Int.* 31:1661–1664. https://doi.org/10.1007/s00296-010-1787-5

Rosengren, S., H.M. Hoffman, W. Bugbee, and D.L. Boyle. 2005. Expression and regulation of cryopyrin and related proteins in rheumatoid arthritis synovium. *Ann. Rheum. Dis.* 64:708–714. https://doi.org/10.1136/ard.2004.025577

Sakurai, H. 2012. Targeting of TAK1 in inflammatory disorders and cancer. *Trends Pharmacol. Sci.* 33:522–530. https://doi.org/10.1016/j.tips.2012.06.007

Segovia, J., A. Sabbah, V. Mgbemena, S.Y. Tsai, T.H. Chang, M.T. Berton, I.R. Morris, I.C. Allen, J.P. Ting, and S. Bose. 2012. TLR2/MyD88/NF-κB pathway, reactive oxygen species, potassium efflux activates NLRP3/ASC inflammasome during respiratory syncytial virus infection. *PLoS One.* 7:e29695. https://doi.org/10.1371/journal.pone.0029695

Shi, H., Y. Wang, X. Li, X. Zhan, M. Tang, M. Fina, L. Su, D. Pratt, C.H. Bu, S. Hildebrand, et al. 2016. NLRP3 activation and mitosis are mutually exclusive events coordinated by NEK7, a new inflammasome component. *Nat. Immunol.* 17:250–258. https://doi.org/10.1038/ni.3333

Sibley, C.H., N. Plass, J. Snow, E.A. Wiggs, C.C. Brewer, K.A. King, C. Zalewski, H.J. Kim, R. Bishop, S. Hill, et al. 2012. Sustained response and prevention of damage progression in patients with neonatal-onset multisystem inflammatory disease treated with anakinra: a cohort study to determine three- and five-year outcomes. *Arthritis Rheum.* 64:2375–2386. https://doi.org/10.1002/art.34409

Snouwaert, J.N., M. Nguyen, P.W. Repenning, R. Dye, E.W. Livingston, M. Kovarova, S.S. Moy, B.E. Brigman, T.A. Bateman, J.P. Ting, and B.H. Koller. 2016. An NLRP3 Mutation Causes Arthropathy and Osteoporosis in Humanized Mice. *Cell Reports.* 17:3077–3088. https://doi.org/10.1016/j.celrep.2016.11.052

Song, N., Z.S. Liu, W. Xue, Z.F. Bai, Q.Y. Wang, J. Dai, X. Liu, Y.J. Huang, H. Cai, X.Y. Zhan, et al. 2017. NLRP3 Phosphorylation Is an Essential Priming Event for Inflammasome Activation. *Mol. Cell.* 68:185–197.

Takeshita, S., K. Kaji, and A. Kudo. 2000. Identification and characterization of the new osteoclast progenitor with macrophage phenotypes being able to differentiate into mature osteoclasts. *J. Bone Miner. Res.* 15:1477–1488. https://doi.org/10.1359/jbmr.2000.15.8.1477

Taylor, G.A., E. Carballo, D.M. Lee, W.S. Lai, M.J. Thompson, D.D. Patel, D.I. Schenkman, G.S. Gilkeson, H.E. Broxmeyer, B.F. Haynes, and P.J. Blackshear. 1996. A pathogenetic role for TNF alpha in the syndrome of cachexia, arthritis, and autoimmunity resulting from tristetraprolin (TTP) deficiency. *Immunity.* 4:445–454. https://doi.org/10.1016/S1074-7613(00)80411-2

ter Haar, E., P. Prabhakar, X. Liu, and C. Lepre. 2007. Crystal structure of the p38 alpha-MAPKAP kinase 2 heterodimer. *J. Biol. Chem.* 282:9733–9739. https://doi.org/10.1074/jbc.M611165200

Tian, J., J.W. Chen, J.S. Gao, L. Li, and X. Xie. 2013. Resveratrol inhibits TNF-α-induced IL-1β, MMP-3 production in human rheumatoid arthritis fibroblast-like synoviocytes via modulation of PI3kinase/Akt pathway. *Rheumatol. Int.* 33:1829–1835. https://doi.org/10.1007/s00296-012-2657-0

Wang, C., C.X. Xu, Y. Alippe, C. Qu, J. Xiao, E. Schipani, R. Civitelli, Y. Abu-Amer, and G. Mbalaviele. 2017. Chronic inflammation triggered by the NLRP3 inflammasome in myeloid cells promotes growth plate dysplasia by mesenchymal cells. *Sci. Rep.* 7:4880. https://doi.org/10.1038/s41598-017-05033-5

Wei, S., H. Kitaura, P. Zhou, F.P. Ross, and S.L. Teitelbaum. 2005. IL-1 mediates TNF-induced osteoclastogenesis. *J. Clin. Invest.* 115:282–290. https://doi.org/10.1172/JCI200523394